PASJ: Publ. Astron. Soc. Japan , 1–??,

Can High Frequency Acoustic Waves Heat the Quiet Sun Chromosphere?

Mats Carlsson[1] Viggo H.Hansteen[1,2] Bart De Pontieu[2] Scott McIntosh[3,4]
Mats.Carlsson@astro.uio.no, Viggo.Hansteen@astro.uio.no, bdp@lmsal.com, mcintosh@boulder.swri.edu
Theodore D. Tarbell[2] Dick Shine[2]
tarbell@lmsal.com, shine@lmsal.com
Saku Tsuneta[5] Yukio Katsukawa[5] Kiyoshi Ichimoto[5] Yoshinori Suematsu[5] Toshifumi Shimizu[6] Shin'ic
saku.tsuneta@nao.ac.jp, yukio.katsukawa@nao.ac.jp, ichimoto@solar.mtk.nao.ac.jp, suematsu@solar.mtk.nao.ac.jp, shimizu@solar.isas.jax
[1]*Institute of Theoretical Astrophysics, University of Oslo, PB 1029 Blindern, 0315 Oslo Norway*
[2]*Lockheed Martin Solar and Astrophysics Laboratory, Palo Alto, CA 94304, USA*
[3]*Department of Space Studies, Southwest Research Institute, 1050 Walnut St, Suite 400, Boulder, CO 80302,*
[4]*High Altitude Observatory, National Center for Atmospheric Research, PO Box 3000, Boulder, CO 80307,*
[5]*National Astronomical Observatory of Japan, Mitaka, Tokyo, 181-8588, Japan*
[6]*ISAS/JAXA, Sagamihara, Kanagawa, 229-8510, Japan*
[7]*Kwasan and Hida Observatories, Kyoto University, Yamashina, Kyoto, 607-8471, Japan*

(Received 2007 June 11; accepted)

Abstract

We use Hinode/SOT Ca II H-line and blue continuum broadband observations to study the presence and power of high frequency acoustic waves at high spatial resolution. We find that there is no dominant power at small spatial scales; the integrated power using the full resolution of Hinode (0.05" pixels, 0.16" resolution) is larger than the power in the data degraded to 0.5" pixels (TRACE pixel size) by only a factor of 1.2. At 20 mHz the ratio is 1.6. Combining this result with the estimates of the acoustic flux based on TRACE data of Fossum & Carlsson (2006), we conclude that the total energy flux in acoustic waves of frequency 5-40 mHz entering the internetwork chromosphere of the quiet Sun is less than 800 W m^{-2}, inadequate to balance the radiative losses in a static chromosphere by a factor of five.

Key words: waves, Sun: chromosphere

1. Introduction

Observations show that the solar chromosphere radiates more than is expected from radiative equilibrium. The extra energy needed to balance the radiative losses must be generated somewhere, transported to the chromosphere and dissipated there. Acoustic waves were suggested early on to play an important role (Biermann 1948; Schwarzschild 1948) because they are readily generated in the convection zone, can easily propagate and are expected to steepen and dissipate in shocks in the chromosphere.

The estimates of the total radiative losses from the solar chromosphere (and thus the required heating) are model dependent. Ulmschneider (1974), Athay (1976) and Vernazza et al. (1981) found the total loss to be 2500-3300 W m^{-2}, 2000-4000 W m^{-2} and 4300 W m^{-2}, respectively. More recently, Anderson & Athay (1989) compared their computed model solar chromospheres with the Vernazza, Avrett and Loeser models and found that the VAL-C model is characterized by a total heat flux of 14000 W m^{-2}, where about 90 % is dissipated near the base of the temperature plateau. The above estimates of radiative losses concerns the average solar chromosphere. For the internetwork regions the losses will be lower, the VAL3A model constructed to fit the lowest intensities observed with Skylab has about 2.2 times lower radiative losses than VAL3C (Avrett 1981).

Carlsson & Stein (1995, 1997) calculated synthetic spectra of the strong chromospheric Ca II H-lines. They showed that the enhanced chromospheric emission, which corresponds to an outwardly increasing semi-empirical temperature structure, can be produced by wave motion without any increase in the mean gas temperature. However, these simulations do not reproduce observations of spectral features formed in the middle to upper chromosphere. The reason could be the lack of waves above 20 mHz in the simulations. On the other hand, high-frequency acoustic waves, even if produced in abundance in the convection zone, are heavily radiatively damped in the photosphere (Carlsson & Stein 2002): at 10 s period only 1% of the generated acoustic energy flux remains at a height of 500 km. In principle, waves with frequencies above what is easily observed from the ground (above 20 mHz) and below what is very heavily damped in the photosphere (below 50 mHz) could account for the energy flux needed to balance the radiative losses from the middle-upper chromosphere where the dynamic models fail. Such waves are by many believed to constitute the dominant heating mechanism of the chromosphere in non-magnetic regions.

The amount of acoustic energy contained in high fre-

quency waves is difficult to determine observationally for two reasons: First, image distortions from the Earth's atmosphere introduces high frequency noise in ground based observations. Second, the width of the intensity formation region of any spectral diagnostic feature smears out the signal of a short wavelength (high frequency) wave in both ground and space based data. Fossum & Carlsson (2005a) showed that the response function of the 1600 Å passband filter of the TRACE (Handy et al. 1999) spacecraft is sufficiently narrow to allow the detection of waves at least up to 40 mHz frequency. Fossum & Carlsson (2005b) used TRACE data to determine the acoustic energy flux of waves in the 5-38 mHz range at the formation height of the 1600 Å passband integrated intensity and found a value of 0.44 kW m^{-2}. A specially optimized observing sequence for TRACE permitted a more detailed study of the acoustic wave power as function of frequency (Fossum & Carlsson 2006): a value of 0.51 kW m^{-2} in the 5-50 mHz range was found (note that the originally published value of 0.255 kW m^{-2} is too low by a factor of two because of an error in a reduction routine). This value is too low by a factor of 4-10 to balance the radiative losses of the internetwork chromosphere as deduced from static models (Avrett 1981; Anderson & Athay 1989). As pointed out in their paper, "The major uncertainty in the analysis is the possibility of high frequency power with spatial scales smaller than the resolution element of TRACE." Cuntz et al. (2007) argues that, indeed, the high frequency power at small scales is sufficient to make acoustic heating of the solar chromosphere locally dominant. They base this conclusion on theoretical calculations of wave power generation, on 1D simulations of acoustic waves (where high frequency waves can account for a temperature increasing with height but where other aspects of the simulation that do not agree with observations have to be attributed to the 1D limitation of the simulation) and on synthetic images from 3D simulations where they refer to the work of Wedemeyer-Böhm et al. (2007). It is obvious that high resolution *observations* would go a long way to answering the question whether a significant acoustic energy flux is hidden in spatial scales smaller than the resolution element of TRACE.

We here present such observations obtained with the Hinode spacecraft at 0.16" spatial resolution (pixel size 0.05"). In Section 2 we present the observations and data reduction, in Sect. 3 we discuss the power spectra of the observations at various spatial scales and we conclude in Sect. 4.

2. Observations and Data Reduction

2.1. Choice of filters and response functions

The TRACE 1600 passband is rather ideal for studying the input of acoustic energy flux into the chromosphere because the response of the passband integrated intensity to perturbations in temperature is not very wide with a weighted mean formation height of 430 km (Fossum & Carlsson 2005a), placing the sensitivity right at the lower boundary of the chromosphere. As pointed out above, the drawback is the large pixel-size of 0.5". With the Solar Optical Telescope (SOT) (Tsuneta et al. 2007) of Hinode (Kosugi et al. 2007) we have a much higher spatial resolution, the diffraction limit ($\frac{\lambda}{D}$) is 0.16" with 0.054" pixel size, but can we find a filter that is sensitive to temperature fluctuations at the lower end of the chromosphere? The prime candidate is the filter centered at the longward of the two resonance lines of singly ionized calcium — the Ca II H-line. This filter is rather wide with an almost Gaussian shape with FWHM of 0.22 nm, so the signal may be dominated by the photospheric wings of the strong absorption line. To investigate the suitability of using Ca II H-line filtergrams for studies of chromospheric dynamics we have determined the intensity response function for the Hinode filter to perturbations of the temperature. We follow the procedure of Fossum & Carlsson (2005a). In general, a response function measures the response of an observed quantity to a given perturbation (Magain 1986). In this case the response function, $R_{I,T}(h)$, measures the response of the relative change in intensity, $\frac{\Delta I}{I}$, given a perturbation in the temperature, $\Delta T(h)$, as function of height in the atmosphere, h. The function is defined from

$$\frac{\Delta I}{I} = \int_{-\infty}^{\infty} R_{I,T}(h) \frac{\Delta T(h)}{T} dh. \quad (1)$$

$R_{I,T}(h)$ is derived numerically from using a step function to introduce a change of 1 % in the temperature of a given reference atmospheric model up to a given point in the atmosphere and varying this point. For each such perturbation, the full non-LTE equations are solved for a six level model atom of Ca II with the code MULTI (Carlsson 1986), the resulting intensity profile of the H-line was multiplied with the Hinode filter transmission profile and integrated and the resulting Hinode intensities were derivated with respect to depth giving the response function. It is obvious that this approach has its limitations — the response is assumed to be linear and we may get a significant contribution from heights where the acoustic waves have actually shocked, violating the assumption of linearity. Furthermore, the derived response function depends on the reference model atmosphere. Nevertheless, such a response function give an indication as to what heights can be diagnosed by intensity variations observed in a given filter.

Figure 1 shows the deduced temperature response function for the SOT/BFI filters Ca II H (centered at 396.86 nm with FWHM of 0.22 nm), G-band (centered at 430.64 nm with FWHM of 0.63 nm), blue-continuum (centered at 450.51 nm with FWHM of 0.23 nm) (all wavelengths in air) using the FALC model of the average quiet solar atmosphere (Fontenla et al. 1990) as reference model atmosphere. It is clear that the Ca II H filter samples the highest regions (average response height of 247 km) while the G-band filter has a photospheric response with a upper photospheric tail (because of the numerous spectral lines in the passband, primarily from CH) with an average response height of 74 km and the blue continuum has a clean photospheric response with an average

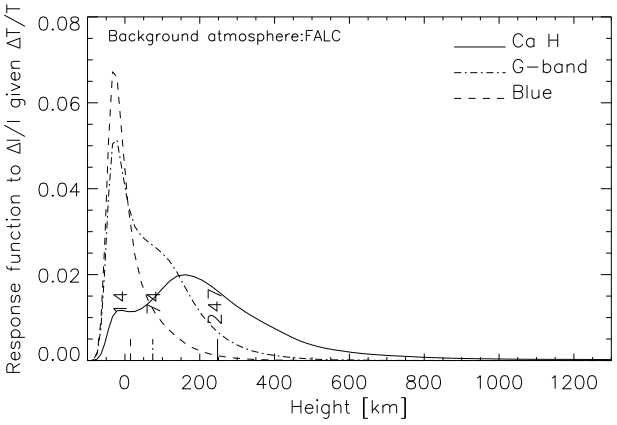

Fig. 1. Response functions for the SOT/BFI filters Ca II H (*solid*), G-band (*dot-dashed*) and blue-continuum (*dashed*) using the FALC model of the average quiet solar atmosphere as reference model atmosphere.

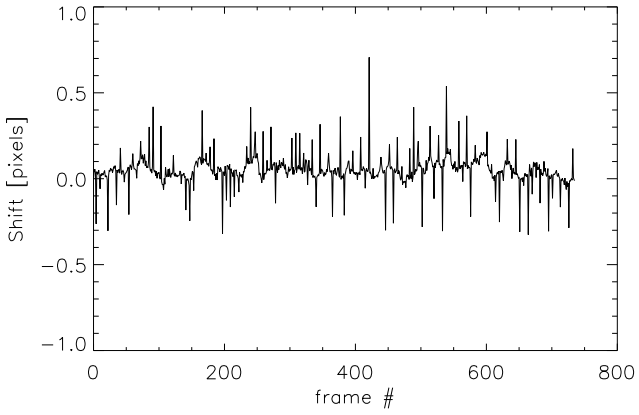

Fig. 2. Residual image jitter after the correlation tracker corrections, calculated from cross-correlation frame to frame.

response height of 14 km. The response function of the Ca II H filter is particularly wide with a long tail extending into the middle chromosphere. The width of the response function will tend to attenuate the response to a wave perturbation — more so for high frequency waves with smaller wavelength. The attenuation as function of frequency of the waves is given by the Fourier transform of the response function (Fossum & Carlsson 2006). For the Hinode calcium filter and the FALC atmosphere we expect very little power beyond 20 mHz (only 5% of the amplitude remains). Note, however, that small scale vertical inhomogeneities would substantially increase the sensitivity to high frequency waves. The blue continuum gives the cleanest photospheric response and has a sharp response function. For this study we therefore choose to observe with high cadence in the calcium filter and the blue continuum filter.

2.2. Observations

The dataset analyzed in detail here was obtained on March 3 2007 between 05:48:03 and 07:09:29 UT and consists of 765 image pairs in the Ca II H filter and the blue continuum filter. The cadence is strictly fixed at 6.4 s with 3.2 s between the blue continuum and the calcium image. We read out only the central 1024x512 pixels of the detector (to keep the high cadence within the telemetry restrictions) thus covering an area of 55"x28" at Sun center. Exposure times were 0.41 s for the calcium images and 0.1 s for the blue continuum. After 736 frames there was a shift in the spacecraft pointing of 12" and we thus restrict the analysis to the first 736 frames in each channel, covering a timespan of $1^h\ 18^m$.

2.3. Data Reductions

We correct the data for dark current and camera artifacts using the IDL routine `fg_prep`, which is part of the Hinode tree of solarsoft (Tarbell et al. 2007). We also need to correct for CCD sensitivity variations by flat-fielding the data. At the time of analysis, there were no flat-field data in the Hinode tree of solarsoft and we therefore constructed our own flat-fields. This was done by extracting all the synoptic observations from disk-center in the period November 2006 to April 2007. Frames that were closer in time than 10 minutes were discarded as were frames containing pores or sunspots. The flat-field was constructed from a mean of the remaining 440 frames. The calcium images have a solar rms variation of 16%. The averaging of 440 independent frames brings this down to an rms variation of solar origin of 0.8%, much smaller than the rms variation of the flat-field image of 3%.

The SOT correlation tracker removes most of the jitter introduced by the spacecraft but visual inspection of the timeseries reveals there is some remaining jitter. This is removed by performing a rigid-co-alignment using cross-correlation from image to image and applying the cumulative offsets to the whole timeseries. Figure 2 shows the deduced image to image shift for the time-series showing that the residual image motion after the correlation tracker corrections is on the order of 0.1 pixels or 0.005" (one standard-deviation). The larger jumps are caused by the replacement of the reference frame of the correlation tracker approximately every 40 s (Shimizu et al. 2007). The shifts calculated from the calcium images and those calculated from the blue continuum images are highly correlated. From this we conclude that the deduced rms is actually uncorrected image motion and not errors in the cross-correlation method. There is drift over the whole timeseries of about 30 pixels or 1.7". This means that there is an area close to the edge of the field of view where we don't have data for the whole timeseries. This area is excluded from the further analysis.

3. Power Spectra

The distribution of power is known to be different in network areas and in internetwork regions. The current dataset is very quiet and does not contain any plage or pore but two small network patches. The area of these patches is so small that the mean power is not affected

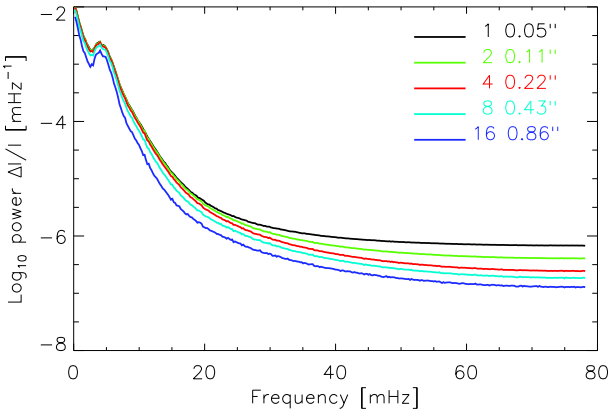

Fig. 3. Power of intensity fluctuations as function of frequency for the SOT/BFI Ca II H filter timeseries at various spatial binnings (colour code in the legend).

whether they are included or not. To facilitate comparisons with various degrees of rebinning, we include the whole area in the following. For each point we calculate the power of the intensity fluctuations relative to the mean intensity ($\Delta I / < I >$) and take the mean. To determine the power as function of spatial resolution, we redo the exercise several times after rebinning the data to 2x2, 4x4, 8x8 and 16x16 original pixels per new pixel.

Figure 3 shows the one-sided power (the power at negative and positive frequencies added together) for the calcium timeseries. Significant power can be seen up to about 30 mHz. The maximum power is at low frequencies, decreasing to 2.5 mHz and then increasing through a local maximum at 4-5 mHz before decreasing again. The noise level goes down with rebinning but very little power is lost by the rebinning at 5-20 mHz: The integrated power in the 5-20 mHz range is 90% of the original value for the data binned to 0.43" pixels and 58% for the data binned to 0.86".

The largest power is at the lowest frequencies. This is probably caused by the granular evolution rather than by waves. We have tried to separate the two components by performing a filtering of the timeseries in the space-time domain with a conical filter. We separate all components that have a horizontal velocity smaller than 7 km s^{-1} (the approximate sound speed) from those with a larger velocity. Sound waves that propagate horizontally should have a phase speed of the intensity signal equal to the sound speed. For an inclined wave, the phase speed will be larger (infinite for a vertically propagating wave). All acoustic waves should thus be contained in the high-pass part of the filtered data while granular evolution (and gravity waves) will be in the low-pass part. Figure 4 shows the original data and the two filtered components for one snapshot. The original data have some intensity modulations of large spatial scale that disappear in the low-pass filtered image (e.g. a dark patch at [10,7] and a bright patch at [2,0]). We find these patches in the high-pass component. It is also clear that the smallest spatial scales are in the low-pass component. Figure 5 shows the same for the blue continuum filter.

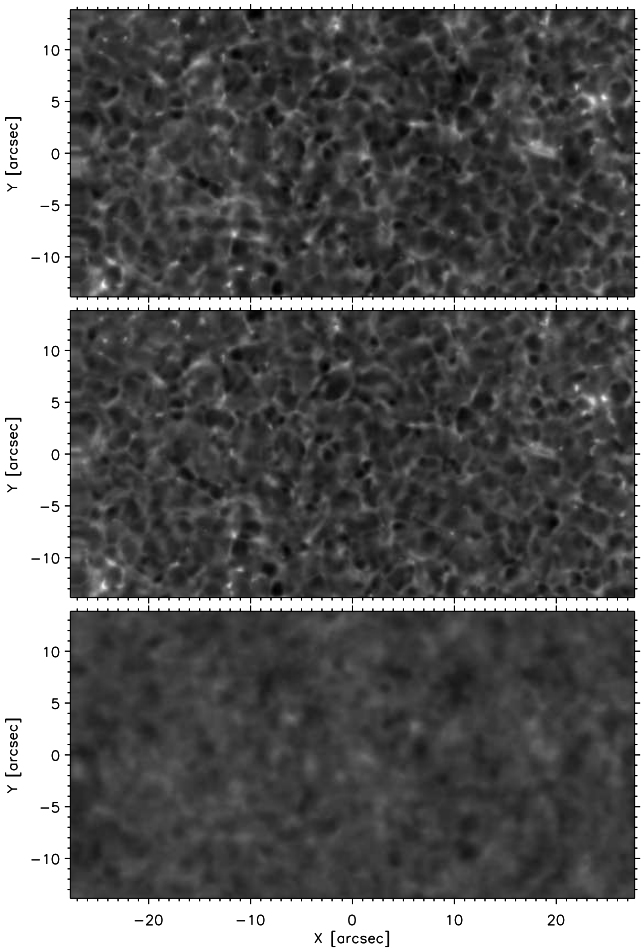

Fig. 4. Ca II H filter image at 06:32:44 UT (*top*), same snapshot with features moving slower (*middle*) and faster (*bottom*) than 7 km s^{-1}.

Figure 6 shows the power in the original data and the two filtered components. The high power at low frequencies is totally dominated by the low-pass component (evolution and gravity waves) while the acoustic wave component gives rise to the peak at 5 mHz and dominates up to 20 mHz. The two components are of equal importance at 30 mHz while the noise is dominated by the high-pass component (where spatially uncorrelated photon counting noise is).

The power of the high-pass filtered data (where we expect the acoustic waves to be) is shown in Fig. 7 which also shows the integrated power in the 5-20 mHz range compared with the 2x2 binned data (we compare with the 2x2 binned data because the unbinned data has high velocity components from alignment interpolations that cancel out when the data is first binned to 2x2. Furthermore, the 2x2 binned data has identical power spectrum as the original data apart from the noise level, see Fig. 3). The power ratios are similar to the case for the unfiltered data except that the high-pass power at low frequencies is identical for the various binnings, showing that the differences at low

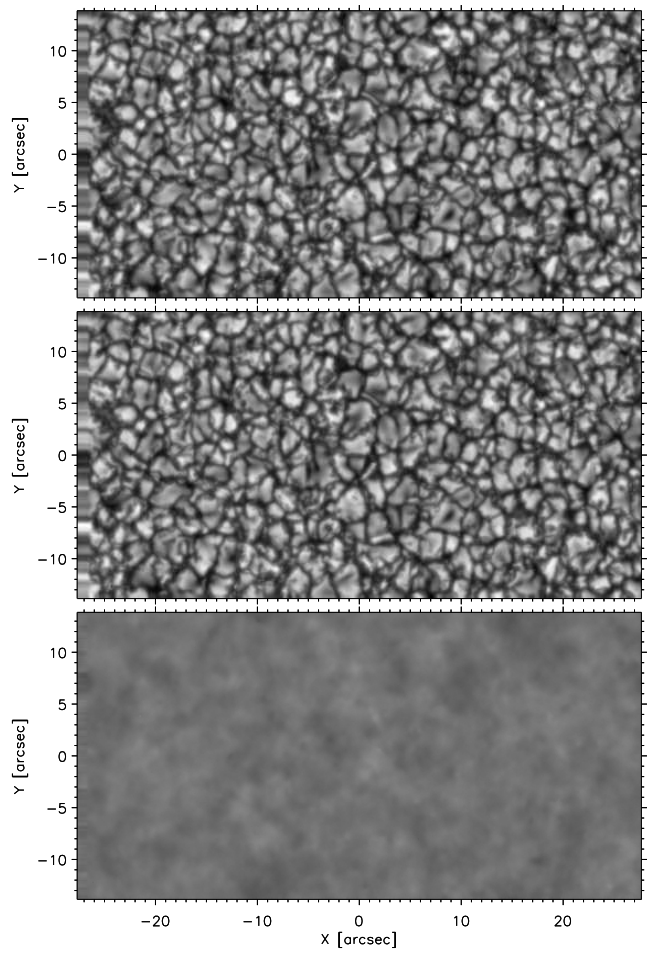

Fig. 5. Blue continuum filter image at 06:32:40 UT (*top*), same snapshot with features moving slower (*middle*) and faster (*bottom*) than 7 km s^{-1}.

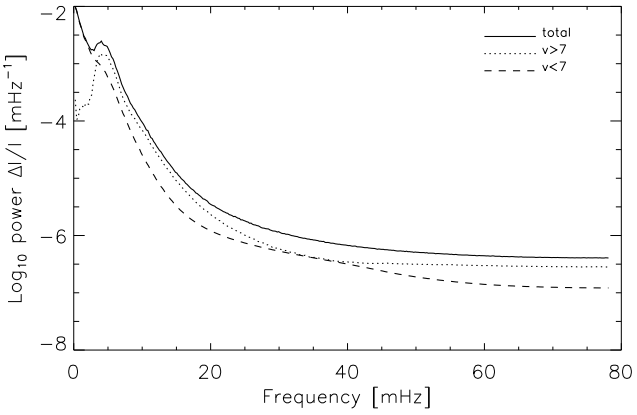

Fig. 6. Power of intensity fluctuations as function of frequency for the SOT/BFI Ca II H filter timeseries (*solid*), for the low-pass filtered component (features moving slower than 7 km s^{-1}) (*dashed*) and for the high-pass filtered component (features moving faster than 7 km s^{-1}) (*dotted*).

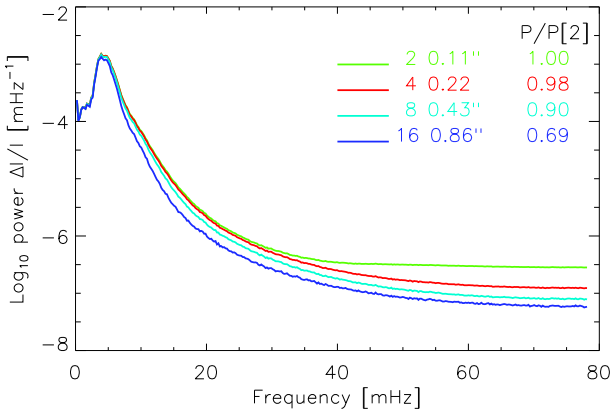

Fig. 7. As Fig.3 but with the data first filtered to remove features that move more slowly than 7 km/s horizontally. The integrated power in the 5-20 mHz range compared with the unbinned data is also given.

frequencies in Fig. 3 are caused by slow motion/evolution of sharp features. The integrated power 5-20 mHz is 90% of the 2x2 binned power at 0.43" binning and still 69% at 0.86" binning. The high percentages are because the integrated power is dominated by the low frequencies close to 5 mHz where the difference between the different binnings is very small. The acoustic power will have a slower decline with frequency because the intensity signal is depressed at higher frequencies from the significant width of the response function (Fossum & Carlsson 2006). One would thus expect that the small spatial scales are more important for the integrated acoustic power than for the integrated intensity power. As an extreme case one can use the ratio of the intensity power at 20 mHz as the ratio for the integrated acoustic power. This ratio is 69% at 0.43" binning and 43% at 0.86" binning.

The Ca II H-line is a scattering line with a broad response function. It could be argued that the spatial scales in the intensity response of this line will be larger than the actual acoustic waves scales and larger than for the TRACE 1600 filter. We have therefore repeated the exercise for the blue continuum that has a much more narrow response function. The response is from the photosphere so we expect the waves to have a much lower amplitude than in the calcium filter. Figure 8 shows this to be the case. The power is lower than for the calcium filter intensities and there is a distinct 3 mHz peak from p-mode oscillations. However, the spatial scales of the high frequency signal is very similar in the two filters: for the blue continuum the integrated power in the 5-20 mHz band is 87% for 0.43" binning and 60% at 0.86" binning. At 20 mHz the corresponding numbers are 65% and 40%, respectively.

For a proper comparison with TRACE, our data should first be smeared with the PSF of TRACE and then rebinned to 0.5" pixel size. The PSF is poorly known but is probably wider than the diffraction limit. The aperture at the 1600 band of TRACE is set by the 11.2 cm diameter of the filter. This corresponds to a diffraction limit of 0.3". TRACE is thus severly undersampled and the

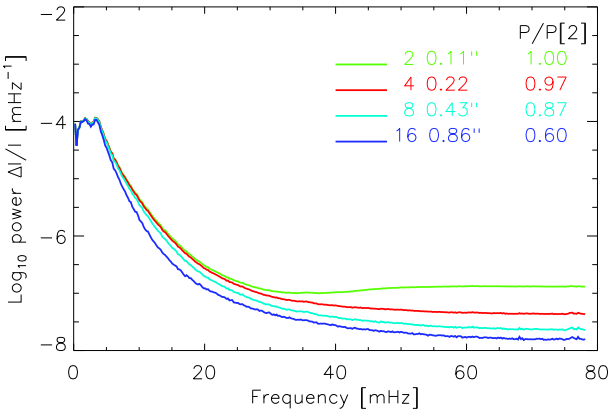

Fig. 8. As Fig.7 but for the blue continuum filter.

PSF would have to be much broader than the diffraction limit to add smearing beyond the pixel sampling. We thus feel that the proper comparison is with the Hinode data rebinned to 0.5". As the numbers above show, even rebinning to 0.86" pixel size does not change the integrated mean power of the timeseries much.

4. Conclusions

We have calculated the power of intensity variations as observed with Hinode SOT/BFI Ca II H and blue continuum filters at high, strictly regular, cadence. We find that intensity power corresponding to propagating acoustic waves is largest close to the acoustic cutoff frequency. Furthermore, the spatial scales of the intensity variations are predominantly larger than the TRACE pixel size of 0.5": The integrated intensity power in the 5-20 mHz range is 83% of the original power when the data is rebinned to the TRACE pixel size. Even at 20 mHz the power of the rebinned data is 64% of the original power. There is no large, unseen, pool of high frequency waves at small spatial scales. Combining this result with the work of Fossum & Carlsson (2005b, 2006) we conclude that the total energy flux in acoustic waves of frequency 5-40 mHz entering the internetwork chromosphere of the quiet Sun is less than 800 W m^{-2}, inadequate to balance the radiative losses in a static chromosphere by a factor of five.

We are grateful to the Hinode team for their efforts in the design, building and operation of the mission. Hinode is a Japanese mission developed and launched by ISAS/JAXA, with NAOJ as domestic partner and NASA and STFC (UK) as international partners. It is operated by these agencies in co-operation with ESA and NSC (Norway). SOT was developed jointly by NAOJ, LMSAL, ISAS/JAXA, NASA, HAO and MELCO. This work was supported by the Research Council of Norway grants 170926/V30 and 170935/V30. B.D.P. was supported by NASA contracts NNG06GG79G, NNG04-GC08G, NAS5-38099 (TRACE) and NNM07AA01C (HINODE). SWM was supported by grants from the NSF (ATM-0541567) and NASA (NNG05GM75G, NNG06GC89G).

References

Anderson L.S., Athay R.G., 1989, ApJ, 346, 1010
Athay R.G., 1976, The solar chromosphere and corona: Quiet sun, D.Reidel Publishing Co., Dordrecht
Avrett E., 1981, In: R.M.Bonnet, A.K.Dupree (eds.) Solar Phenomena in Stars and Stellar Systems, p.173, D.Reidel Publishing Co., Dordrecht
Biermann L., 1948, Zeitschrift fur Astrophysics, 25, 161
Carlsson M., 1986, A Computer Program for Solving Multi-Level Non-LTE Radiative Transfer Problems in Moving or Static Atmospheres, Report No. 33, Uppsala Astronomical Observatory
Carlsson M., Stein R., 1995, ApJ, 440, L29
Carlsson M., Stein R., 1997, ApJ, 481, 500
Carlsson M., Stein R.F., 2002, In: Proc. of the Magnetic Coupling of the Solar Atmosphere Euroconference and IAU Colloquium 188
Cuntz M., Rammacher W., Musielak Z.E., 2007, ApJL, 657, L57
Fontenla J.M., Avrett E.H., Loeser R., 1990, ApJ, 355, 700
Fossum A., Carlsson M., 2005a, ApJ, 625, 556
Fossum A., Carlsson M., 2005b, Nature, 435, 919
Fossum A., Carlsson M., 2006, ApJ, 646, 579
Handy B.N., Acton L.W., Kankelborg C.C., et al., 1999, Sol. Phys., 187, 229
Kosugi T., et al., 2007, Solar Physics, (to be submitted)
Magain P., 1986, A&A, 163, 135
Schwarzschild M., 1948, ApJ, 107, 1
Shimizu T., et al., 2007, Solar Physics, (submitted)
Tarbell T., et al., 2007, Solar Physics, (to be submitted)
Tsuneta S., et al., 2007, Solar Physics, (to be submitted)
Ulmschneider P., 1974, Sol. Phys., 39, 327
Vernazza J.E., Avrett E.H., Loeser R., 1981, ApJS, 45, 635
Wedemeyer-Böhm S., Steiner O., Bruls J., Ramacher W., 2007, In: Dorotovic I., Heinzel P., Rutten R. (eds.) Physics of the Chromospheric Plasmas, ASP Conference Series, vol. 368